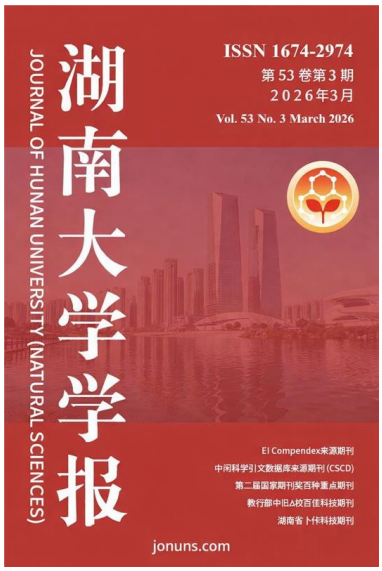

Journal of Hunan University

(Natural Sciences)

Vol. 53 No. 3

March 2026

Available online at

https://jonuns.com

Open Access Article

https://doi.org/10.55463/issn.1674-2974.53.3.2

Implementation of a Deep Learning Estimation Model for Identifying Induced Failure Hazard Areas in Construction Equipment

Labanyo Bacher*[1], Linqi Huang[1] , Hasan Md Mehedy[2] , Protiva Sarkar[1]

[1] School of Resource and Safety Engineering, Central South University, Changsha, China,
[2] Department of Mechanical Engineering, Hubei University of Technology, Wuhan, China,

* Corresponding author: 235518007@csu.edu.cn

Article History:

Received: January 29, 2026
Revised: February 27, 2026
Accepted: March 8, 2026
Published: March 31, 2026

Abstract: Overturning accidents involving heavy construction vehicles may occur due to soft ground conditions caused by subsurface water accumulation or sinkholes. Although such accidents may appear unexpected during visual inspection, subsurface failure often precedes these events. Therefore, real-time assessment of ground stability is essential for improving operational safety.

Electrical Resistivity Tomography (ERT) is a widely used geophysical method for analyzing subsurface conditions through deep ground investigation. However, ERT data interpretation typically involves complex nonlinear inversion processes that are computationally intensive and highly dependent on initial parameter estimates.

In this study, an inference-based deep learning approach is proposed to efficiently identify areas susceptible to overturning accidents. The method converts data obtained using a Wenner array configuration into a high-resolution dipole–dipole configuration, thereby eliminating the need for traditional inversion procedures.

To evaluate the performance of the proposed framework, three deep learning models—Multi-Layer Perceptron (MLP), Convolutional Neural Network (CNN), and Long Short-Term Memory (LSTM)—were trained and tested using regression-based loss functions. Among these models, the MLP demonstrated the best performance, achieving an average R^2 value of 0.9935 ± 0.0014 and a root mean square error (RMSE) of 3.44%.

The proposed approach leverages the inherent stability of the Wenner array and the high spatial resolution of the dipole–dipole configuration. By employing forward inference, the method significantly reduces the computational

complexity associated with conventional inversion techniques. As a result, the efficiency and practical applicability of ERT-based ground inspection are substantially improved.

Overall, the proposed framework provides an effective tool for identifying hazardous ground conditions and assessing the susceptibility of construction sites to overturning accidents involving heavy vehicles.

Keywords: Deep learning; electrical resistivity tomography; ground stability assessment; construction equipment safety; overturning accident prediction; machine learning models; subsurface hazard detection.

施工设备诱发失效危险区域识别的深度学习估计模型实现

摘要：由于地下积水或塌陷等因素导致地基软化，重型施工车辆在作业过程中可能发生倾覆事故。尽管此类事故在表面观察中往往难以提前发现，但地下结构失稳通常是事故发生前的重要征兆。因此，对地基稳定性进行实时评估对于提高施工安全性具有重要意义。

电阻率层析成像（Electrical Resistivity Tomography, ERT）是一种广泛应用于地下结构探测与地基条件分析的地球物理方法。然而，ERT 数据解释通常依赖于复杂的非线性反演过程，该过程计算成本高且对初始参数估计具有较强依赖性。

本研究提出了一种基于推理机制的深度学习方法，用于高效识别易发生倾覆事故的危险区域。该方法通过将 Wenner 阵列获取的数据转换为高分辨率的偶极—偶极（Dipole–dipole）阵列数据，从而避免了传统反演过程的需求。

为了评估所提出方法的性能，构建并比较了三种深度学习模型：多层感知机（MLP）、卷积神经网络（CNN）和长短期记忆网络（LSTM），并采用回归损失函数进行训练与测试。实验结果表明，MLP 模型表现最佳，其平均决定系数 R^2 达到 0.9935 ± 0.0014，均方根误差（RMSE）为 3.44%。

该方法充分利用了 Wenner 阵列的稳定性以及偶极—偶极阵列的高空间分辨率优势。通过采用前向推理机制，该方法显著降低了传统反演技术带来的计算复杂度，从而提高了基于 ERT 的地基检测效率与工程应用可行性。

总体而言，本文提出的框架为识别危险地基条件以及评估施工现场重型车辆倾覆事故风险提供了一种有效工具。

关键词：深度学习；电阻率层析成像；地基稳定性评估；施工设备安全；倾覆事故预测；机器学习模型；地下灾害识别

1. Introduction

Medium to large-sized earth-moving machinery using outriggers is employed for transporting heavy loads and is a basic requirement in the construction industry. But the use of earth-moving machinery invites the risk of overturning accidents. These accidents may result in serious injuries and property loss in an industrial environment. [1,2,3] Since overturning accidents due to soft ground like groundwater or sinkhole collapse occur rapidly compared to those caused by the failure of the machinery itself, as well as the carelessness of the operators or heavy loading, collapse above the ground takes place slowly from a distance. It is not easy to detect. [4,5] There is a requirement for a technology capable of qualitatively evaluating the ground conditions online and determining the dangerous regions beforehand.

The types of geophysical explorations available to diagnose anomalies on earth are mostly non-destructive surveys of the ground. [6] Examples of geophysical explorations are Electrical Resistivity Tomography (ERT), which carries out calculations of electrical resistivity by passing current into the earth using electrodes; Electromagnetic (EM), which makes use of mobile electromagnetic waves and electromagnetic radiation; and Ground Penetrating Radar (GPR). [7] ERT, EM, and GPR are more adaptable to soft ground surveys compared to other explorations. [8] Among

ERT, EM, and GPR explorations, ERT has the ability to detect properties of wide and deep regions of the earth. In this measurement, there are disadvantages such as the current path and current distribution that are not linear. Moreover, complex data mapping of the measurement location and inversion analysis are required. In contrast to ERT, EM and GPR have easier measurements compared to ERT and are done on a wide area at a short period of time. The measurement, however, has limited depth of only 3 m. Moreover, interpretation of data from measurement requires consideration of metallic materials and electromagnetic interference or noise, and data processing using modeling or filtering, especially when measuring high moisture content in soft soil.

A data inference model using deep learning for the proposed research aims to overcome the limitations of data analysis in ground exploration by efficiently recognizing suspect areas that are likely to tip over because of the presence of construction machinery. For this purpose, we employed the use of ERT, since the method can perform deep-depth exploration, unlike EM and GPR, which are restricted to shallow depths only. In this case, the objective was to augment the nonlinearity of the generated data by the electrode configuration using a deep learning model for inference. Namely, the low-resolution ERT, with its expertise in vertical exploration, was used for the inference of high-resolution ground information using deep learning models for data transformation.

2. Existing Research and Differentiation

2.1. Traditional Numerical Analysis-Based Inversion Studies

Electrical resistivity data analysis is a complex process due to presence of nonlinearities because of electrode configurations, ground resistivity patterns, and noise. The conventional inversion techniques with strong roots in numerical analysis have been predominantly used in previous studies. [9] In this inversion technique, a primitive earth model is formulated by measurement of voltage differences among electrodes. Then, this earth model is successively altered to minimize discrepancies between observations and theoretical predictions. Unfortunately, this process is fraught with instabilities because solutions significantly depend on the initial model to be used. Moreover, this inversion process modeled currents nonlinearly because their paths depend upon whether current is injected in a specific manner or according to specified electrode configurations. In reality, this process still relies upon linear currents approximately. The iterative optimization process is rather demanding in computation because of high overhead costs due to increased time complexity. In this context, presence of environmental factors, for instance, ground resistivity variations due to soil properties, humidity, and ground temperatures, significantly alters paths of currents and their decay patterns. [10] Unfortunately, numerical analysis-based inversion procedures have difficulties in taking care of these factors. In this context, different people interpret similar data differently because of specific initial earth model choices depending upon their personal judgment. This makes soil structure analysis rather ambiguous.

2.2. Research on Deep Learning-Based Inversion Correction

However, in order to overcome the limitations that traditional approaches to inversion have, a lot of research has been carried out recently concerning the application of deep learning tools to the interpretation of electrical resistivity data. Deep learning algorithms are strong at fitting non-linear equations, hence capable of detecting interactions in the data that traditional models are not. The main goal of early works has been to overcome the non-linear characteristics which become visible in the process of inversion and improve the accuracy and robustness of the interpretation, through a variety of architectures of the neural networks like the Convolutional Neural Networks, the U-Net, the auto-encoders, and Deep Neural Networks. [11, 12, 13]

For example, high-resolution reconstructions of the potential field between electrodes have been achieved using CNN- and U-Net-based models on 3D modeling, allowing us to localize where and how the electrical responses change with depth. Furthermore, low-dimensional spatial reparameterization using autoencoder learning resulted in noise-resilient representations of the data, and optimization on spatial mapping solved inverse problems with details that are not possible with traditional inversion schemes due to learned non-linear patterns from electrode or earth changes. However, most of the present research is concerned with steps in the postprocessing part for correction of non-linearities in inversions. In fact, they frequently overlook the structural non-linearities inherent in the original date, caused by the natural properties of the electrode array. In other words, these models do not learn how the signal decay, current flow, or noise resilience evolves in different electrode arrays, such as Wenner or Dipole-Dipole arrays.

2.3. Problems with Existing Research

The selection of the type of electrode arrays in the electrical resistivity technique is greatly responsible for the interpretation of the results because different electrode arrays follow different principles of measurement and provide different values of exploration resolution. [14] Wenner arrays allow equal spacing of the current and potential electrodes; therefore, they produce a more stable current path and better signal-to-noise ratios. However, the close spacing of the electrodes is responsible for the inability of the Wenner arrays to produce better exploration results in the deep

sea. Additionally, the dipole-dipole arrays separate the current and potential electrodes; therefore, they are able to explore the deep sea more compared to other arrays. However, an increase in the distance of the electrodes in order to explore deeper targets leads to decreased signal strength and increased susceptibility to noise in the data collection process. Similarly, for the same type of arrays, the current flow pattern and changes in the voltage follow very different principles depending upon the ground porosity, moisture content, temperature, and geological formations of the environment; therefore, the results of the electrical resistivity technique are more nonlinear in nature. Inversion methods currently available through numerical analysis and correction by means of deep learning approaches are not capable of appropriately capturing the intrinsic structural properties of electrode arrays as well as nonlinearities involved in data generation. Such shortcomings directly contribute to reduced resolution, distortions in data, and poor generalization of models. There arises a need for a new paradigm of data analysis that has the ability to foresee nonlinearities involved in data generation by means of every electrode array.

2.4. Distinctiveness of the Proposed Study

In order to break through the barriers, set by existing research, this research proposes a cross-map approach using deep learning, which takes Wenner array data as the input and provides high-resolution results on the dipole-dipole array. The proposed approach is centered on learning, in a straightforward and upfront manner, the existing structural non-linear relationships between electrode arrays, followed by their immediate correction in the raw data phase. Even as it seeks to maintain the integrity of the signal, it hopes to enhance exploration resolution, all this in a bid to cut the costs in the course of optimization. Through its ability to learn high-dimensional representations, it is able to eliminate noise in a better manner, thereby improving the signal-to-noise ratio.

In particular, the differences mentioned in Table 1 regarding Wenner and dipole-dipole electrode configurations involve more than simple differences in measurement. These differences form the crux of identifying the essential sources of the nonlinearity that lie hidden in the measurements. While the Wenner array ensures high-quality measurements based upon robust signal stability and high noise immunity, the resolution is not conducive to identifying intricate geological formations. Conversely, the dipole-dipole array ensures high-resolution geological formations but may be susceptible to noise.

Table 1. Comparison of Wenner and Dipole-dipole arrays in electrical resistivity tomography

Category	Wenner	Dipole-dipole
Signal attenuation	Attenuates as electrode spacing increases	Attenuates as spacing between current and potential electrodes increases
Current path distribution	Nonlinear diffusion primarily in the vertical direction	Nonlinear diffusion primarily in the horizontal direction
Sensitivity orientation	Higher sensitivity in the vertical direction	Higher sensitivity in the horizontal direction
Signal-to-noise ratio	Relatively high and stable	Relatively low and more susceptible to noise
Distortion in heterogeneous media	Signal distortion at layered boundaries	Signal distortion in complex heterogeneous structures
Resolution	Low (fewer independent measurements)	High (larger number of independent measurements)
Depth response	Relatively stable but decreases with depth	Strong nonlinear variation with increasing depth
Typical application environment	Suitable for relatively homogeneous subsurface conditions	Suitable for imaging complex or heterogeneous geological structures

Looking simultaneously at the alluvial features and integrating the way and means of the two sets in relation to one another, the model can correct the non-linear issues that had previously gone unconsidered, right in the source of the data.

3. Research Methods and Model Construction

This work extends the previous electrical resistivity-driven approach to the prevention of tipping in construction equipment and its related data-analysis methods. [15,16] We enhance the existing framework by creating simulated datasets that reflect a variety of ground structures, and we tie these datasets to a deep-learning inference model. In this paper, I outline in detail the preprocessing steps of the data, the model design, the training process, and the evaluation for the deep-learning pipeline.

We introduce, in particular, a deep-learning model that takes low-resolution Wenner data as input and provides high-resolution dipole-dipole responses as output, from 10,000 simulated pairs of Wenner and dipole-dipole resistivity measurements. We will combine the architecture of an MLP with that of a CNN and an LSTM network to evaluate and compare the predictive performance of different ground-condition scenarios. Our aim is to provide efficient inference about ground conditions with as little use of complex numerical inversion as possible.

3.1. Dataset Composition and Preprocessing

Real-world ERT data acquisition falls through due to extensive variations within the ground materials and environments. To create a deep learning dataset, we utilized ResIPy [17] and Python [18] tools for modeling and inversion of electrical resistivity surveys. These simulations imitated various structural variations in the ground, with softer surfaces and a wide range of electrical conditions, each based on the geometry of the

ERT electrodes. The ground model was randomly generated to decide how many objects there are, where they sit, how big they are, and what their electrical resistivity is, so the synthetic data captures the heterogeneity and complexity seen in real geologies and various exploration scenarios. A discrete uniform distribution was used in order to keep the generated data statistically balanced and not biased toward particular cases. Ground geometry was created as models with one, two, or three anomalies, shown in Figure 1. The resistivity of background soil was randomly chosen between 200 and 500 ohm-meters, the usual range for soil, while each object's resistivity was drawn from 1 to 1000 ohm-meters, representing soft ground such as groundwater pockets or cavities. Uniformly sampled within their respective ranges were the sizes and locations of the objects. A key step was enforcing physical plausibility: we checked for overlaps and adjusted object positions such that they would not intersect. This approach, combining both random and uniform distribution with overlap checks, creates a dataset that helps the deep learning model generalize across a wide variety of conditions rather than favoring a narrow set of scenarios.

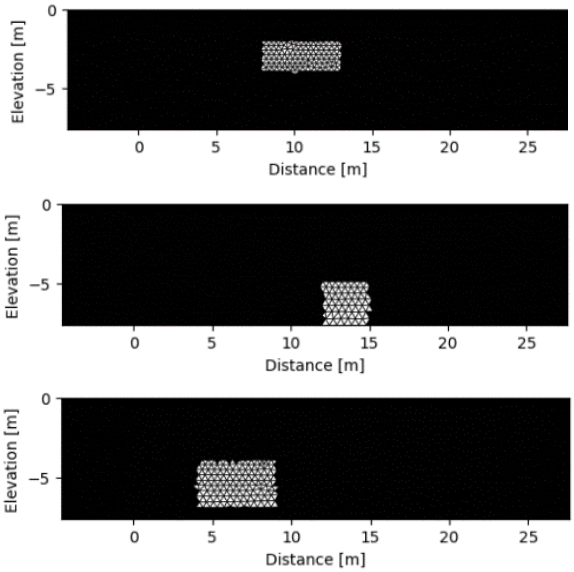

(a) Subsurface model with one anomaly object

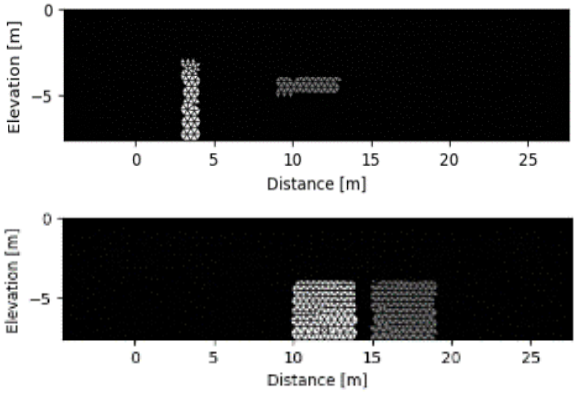

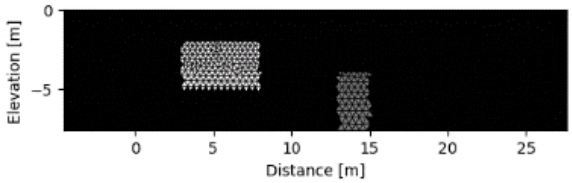

(b) Subsurface model with two anomaly objects

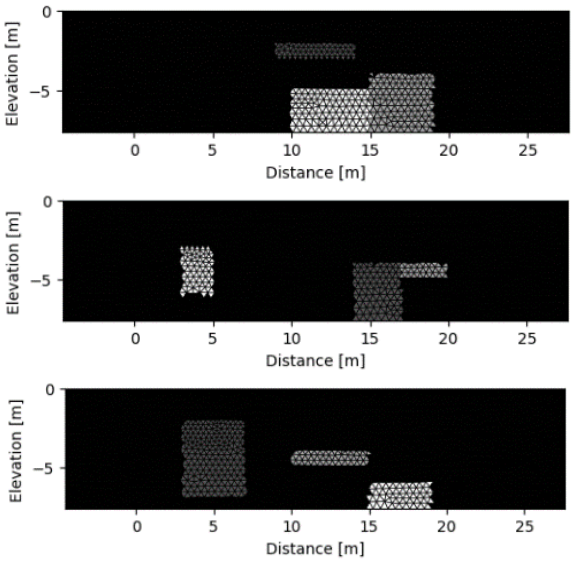

(c) Subsurface model with three anomaly objects

Fig 1. Geological example simulated for training deep learning models

The simulation data came from modeling how electrical resistivity would respond for each ground model, using the Wenner and Dipole-dipole configurations on a 24-electrode layout defined in an earlier study. With that array, Wenner offers 84 valid measurement combinations, while Dipole-dipole offers 231. This gap stems from how each method places current and potential electrodes and the depth ranges those placements tend to probe. [19] In this work, we ran 10,000 simulations and produced data pairs for every ground model using both Wenner and Dipole-dipole setups. The results were organized into one-dimensional vectors arranged by exploration depth and the spatial ordering dictated by each array, forming a dataset suitable for deep learning. The ground models were generated randomly from a discrete uniform distribution, with each model containing roughly one-third of the objects shown in Figure 1.

Electrical resistivity survey data, categorized by electrode pattern, is applied to the experiment. Regarding the Wenner configuration, the data is arranged in a 1D vector form with 84 elements, defining 10,000 simulation points, thereby creating a 10,000-by-84 input matrix. The dipole-dipole configuration takes the same procedure but with a 231-element 1D vector, hence creating a 10,000-by-231 target matrix because it also involves the same 10,000 simulation points. In total, there are 10,000 Wenner-dipole-dipole data pairs.

The data split process allocates 70% to training, with 15% allocated to both validation and testing, with

randomization to allow reproducibility. [20] The initial process of data splitting sets aside 30% of data to create a temporary dataset, with the other 70% labeled as the training dataset. The temporary dataset of 30% is split evenly into two sections to be labeled as either a validation set or a test set. This ensures that data reproducibility occurs through random splitting of data to combat overfitting.

3.2. Deep Learning Model Design and Training

In this case, we have designed a deep learning model based on a data transformation process. The model takes electric resistivity values in a Wenner array as an input and tries to predict the values of a dipole-dipole array. The model tries to represent the nonlinear relationships among various electrode array combinations and has been designed to transform a 1x84 output of the Wenner array into a 1x231 dipole-dipole array. In this case, we have used the MLP model, a CNN model, and an LSTM model to compare their effectiveness. There are four hidden layers in the MLP, each fully connected from the input to the output layer. Each neuron conducts high-dimensional function approximation by using linear functions followed by activation functions, attempting to find the mapping from the electrode configuration. The CNN uses a one-dimensional convolutional network. It processes the Wenner data as a sequence in 1D to identify the corresponding patterns in the data in order to predict the dipole-dipole response. Finally, the fully connected layer is used for the regression output since the data is continuous in the spatial dimension. The LSTM utilizes a recurrent architecture that considers the sequential relationships in the Wenner data through internal cell memory within the model to account for the long dependencies in the data.

Deep learning models were compared with respect to performance using the size of the primary hidden layer, which involved the addition of the number of neurons. The models were similar in magnitude in the amount of information that can be learned, as the same parameters were maintained in the experiment: the rate at which the models were trained, the epochs, the size of the batch, the optimizer, the loss, and the activation functions. The structural differences were evaluated without the influence of other factors that may impact performances. There are a number of reasons why hidden layer neuron numbers are specifically highlighted. Firstly, hidden layer neuron numbers are a key component of model expressiveness, or expressive power, with more complex model functions able to be expressed through a balanced neuron number to eliminate underfitting and overfitting. [21,22,23] Secondly, hidden layer neuron numbers are particularly informative when comparing models with architectures such as MLPs, CNNs, or LSTMs. The scalability of neuron numbers allows model complexity to be easily understood. Even if other parameters change, hidden layer neuron numbers offer a clear understanding of model parameters. [24] Thirdly, hidden layer neuron numbers are specifically associated with model efficiency of computation. [25] In other words, hidden layer neuron numbers have the potential to dramatically increase computational costs if increased, such that growth allows researchers to identify computational costs. Lastly, most current frameworks and research on AI models define artificial models with hidden layer neuron numbers, such that model communication and reproducibility of current research are possible. [26] In order to make fair comparison among them, the structure of MLP, CNN, and LSTM was designed layer by layer based on the number of hidden neurons these networks contain. The aim was to ensure that overall learning parameters remain relatively equal among competing models. There were approximately 540,000 learning parameters in the MLP structure, approximately 550,000 learning parameters in CNN structure, while approximately 510,000 learning parameters were in the LSTM structure. The number of hidden neurons in respective networks was appropriately adjusted. The network architecture details along with respective training hyper-parameters of deep learning models are provided in Table 2. The variations among these architectures are their unique characteristics. By retaining hyper-parameters constant among identical conditions, variations in their performances due to the change in number of neurons were properly analyzed.

3.3. Model Performance Evaluation Metrics

In order to effectively evaluate generalization and learning on deep learning models, the current research utilized analysis of loss curves and regression performance metrics. The model being a regression model predicting dipole-dipole array response from Wenner array data, it becomes imperative to consider evaluation metrics that consider the actual data's resemblance to model predictions.

We started by inspecting the loss curve in a manner that helps in understanding the learning process being followed by the model over a period of time, including whether it results in overfitting. A typical indicator for overfitting in a loss curve is if it is noticed that the training loss is decreasing, but from a point, the validation loss levels off or increases. In our case, we checked for generalization by observing whether the loss curve is stable, where it should decrease in the beginning but become stable over a period of training. We evaluate the performance of the regression model using three statistics: (R^2), MSE, and RMSE. (R^2) describes the proportion of the variability of the real values that is captured by the model's predictions. An (R^2) close to 1 implies a high explanatory power for the model. MSE calculates the average of the squared errors between predicted and actual values; this provides a

simple and interpretable sense of how wrong the predictions tend to be. RMSE computes the square root of these mean-squared errors, making it sensitive to big mistakes in a way that aids in diagnosing large-scale failures in prediction. These metrics together describe the deviation of the model's inferred targets from the true targets quantitatively and provide a few angles with which to view the performance of the regression.

Table 2. Summary of deep learning architectures and hyperparameters

Model Structure / Hyperparameter	MLP	CNN	LSTM
Architecture	Fully connected layers	Convolutional layers for spatial feature extraction	Recurrent layers with memory cells for sequential data
Input Dimension	1 x 84 vector (Wenner)		
Output Dimension	1 x 231 vector (Dipole-dipole)		
Hidden Layer (units per layer)	4 layers (128, 256, 512, 512)	3 layers (64, 128, 256)	1 layer (256)
Activation function	ReLU (Rectified Linear Unit)		
Loss Function	MSE (Mean Squared Error)		
Optimizer	Adam (Adaptive Moment Estimation)		
Learning Rate	0.001		
Epoch	100,000		

The model truly infers, to a large extent. We have done a visual side-by-side check: input Wenner data, target Dipole-dipole values, and the model's own inferred Dipole-dipole results drawn from Wenner. It was learned by the network to faithfully reproduce the Wenner measurements of response traits of a dipole-dipole array, while inferred dipole-dipole outputs showed a distribution and pattern close to real targets. This comparison was a qualitative cue that the model had picked up structural relationships between the two array types, not just some rough numerical fit.

4. Inference results of the deep learning model

4.1. Learning Performance and Convergence Characteristics of Deep Learning Models

For each model's performance evaluation, the training was followed through the curves shown in Fig. 2. Training was carried out to 100,000 epochs. When the minimum mean squared error was 0.00005 or lower, or when there was no improvement in the validation loss during a number of epochs, early stopping was triggered.

In MLP model (Figure 2(a)), the initial values of the loss were relatively higher, but after around 400 epochs, the loss values became stable and dropped to less than 0.02. The difference between the values of training and validation remained small, thus showing proper generalization of the process of input and output.

The CNN model (Fig. 2(b)) also learned faster, as the loss decreased rapidly, and after approximately 500 epochs, both training and validation loss decreased below 0.001. The similar convergence pattern for both training and validation sets with the CNN model suggests that the network was effective in capturing the spatial pattern information in the apparent resistivity data.

In case of LSTM models (Fig. 2(c)), the converging process was also smooth, where the training as well as validation loss remained below 0.0005 for approximately 100 iterations. LSTM performed satisfactorily in understanding the temporal relationships between the input patterns.

In short, the results of all three models indicated a strong initial drop in the loss function followed by the convergence of the loss function. Both CNN models and the LSTM model were able to achieve lower losses compared to the MLP model. Additionally, the difference between the training loss and the validation loss was negligible.

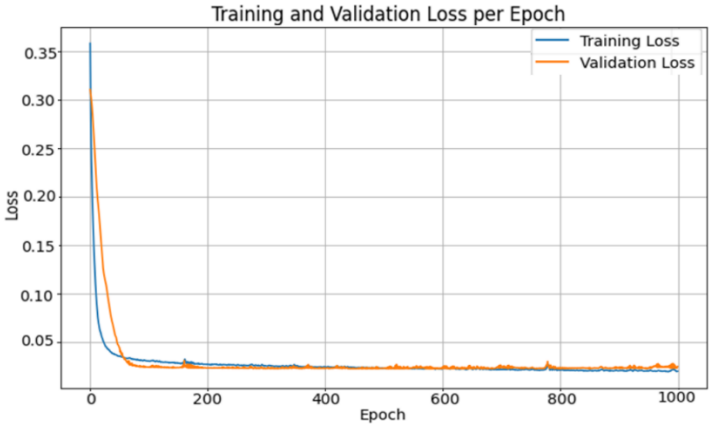

(a) Multi-layer perceptron

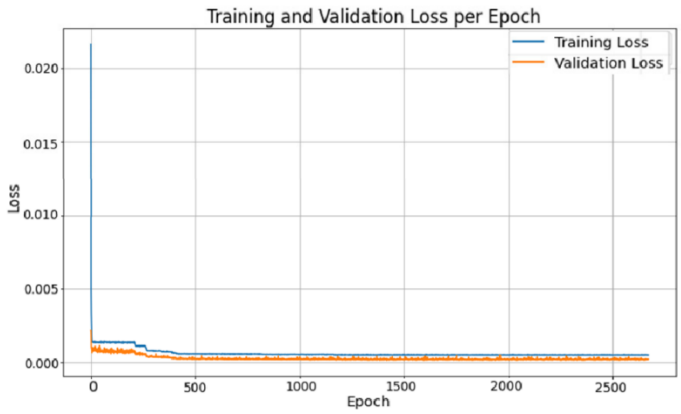

(b) Convolutional neural network

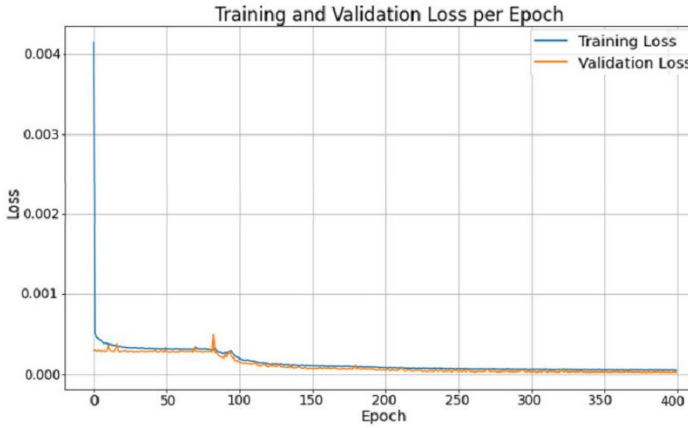

(c) Long short-term memory

Fig 2. Comparison of training and validation loss curves for the proposed MLP, CNN, and LSTM models

4.2. Inference Performance Evaluation by Deep Learning Model

The proposed MLP, CNN, and LSTM models' prediction accuracy on the test set has been analyzed using R^2, MSE, RMSE, and relative error rate. When the predicted values were compared to the corresponding targets on the same set of data, the three models performed well on the regression tasks, as they all had an R^2 of over 0.95: MLP = 0.9949, CNN = 0.9474, and LSTM = 0.9782. However, in drawing inferences from one observation, due consideration has to be given to the random elements that exist in certain aspects, such as weight initialization, shuffling of the datasets, and dropout in the process of model training, which could result in variations in the inferences, despite the setup looking the same and different setups having different inferences. To compensate for the above, the three models have been trained for a minimum of 10 instances under the same setup, and the mean and standard deviation between the R^2 and MSE values have been calculated." "The mean values of the three models on R^2 and MSE were MLPR^2 = 0.9935 ± 0.0014, CNNR2 = 0.9493 ± 0.0025, and LMBR^2 = 0.9774 ± 0.0012, respectively, and the three had remarkably low values for the standard deviations, signifying that.

In the case of one-dimensional structured data, it is most important to recognize that it is necessary to extract the complex nonlinear relationships between data elements rather than extracting spatial and temporal features. In this scenario, Multi-Layer Perceptrons (MLP) are most appropriate, which provide an easiest and most efficient solution for learning these patterns. Even then, MLP-based models demonstrate the highest average R^2 value and feasibility in terms of fast learning, fast processing, and efficiency. Conversely, the Convolutional Neural Networks (CNNs) are robust in the case of one-dimensional data. However, their application in the processing of the Wenner and Dipole-dipole array data into an exploitable form in this case appears limited. This is most likely due to the robustness of CNNs in local feature detection, which appears less important compared to the global nonlinear mappings that the MLP has captured in the dataset. Also, the filter sizes employed appear less effective in capturing the characteristics of the dataset. Regarding Long Short-Term Memories (LSTMs), their capability in sequence identification is not utilized to the full, as it does not actually map to a temporal order in the measurement values. Perhaps the long-term dependency part overfit the map relationships already embedded in the data.

From the analysis, the MLP was selected as the inference model of choice. In order to calculate the numerical efficiency of how well it performed, the average error was determined. The average target value was given by 208.95 Ω·m, while that of the average predicted target was 208.98 Ω·m, with almost parallel movements. The model's mean squared error was estimated at 51.79 with a Root Mean Squared Error of 7.2, with a relative error rate of approximately 3.44% from RMSE. This verification analysis validates that the MLP inference model has been able to make accurate predictions of the electrical resistivity of real soft soil.

4.3. Visual Analysis of Data Inference Results

In this section, we carried out a qualitative visual analysis task on the inference results for the MLP model using the same set of 1,000 new pairs. We established three baseline models according to the number of anomalies seen in the ground in one, two, and three objects. We compared the prediction results for the dipole-dipole using the Wenner array's input with the raw target values.

In the single-object configuration (see Fig. 3(a), (b)), the model field includes a small resistivity anomaly within a thick background, modeling the soft ground environment with the presence of ground water, Darcy flow, having very low resistivity values. However, the MLP model-generated dipole-dipole response corresponding to this ground setup matches the target response quite closely, including the locations and values of the prominent peaks of the resistivity factors. Even the nonlinear characteristics, such as the abrupt variation in the resistance values at the center, are represented very effectively. This indicates the model, in effect, is not simply performing direct numerical mapping; instead, the model identifies the remarkable characteristics of the dipole-dipole response configuration.

In the multi-object scenario (Fig. 3(c), (d)), the ground conditions were simulated as soft earth, characterized by two objects showing different resistance properties. In this case, the MLP method was able to record the overall waveform characteristics of the dipole–dipole measurements, but some incongruities appeared in the peak positions and amplitude overestimation. This may be attributed to the complex electrical coupling patterns

among the two objects being transferred to the Wenner array's input variables in such a manner that it was not straightforward for the model to identify the individual effect.

In the complex subsurface structure (refer Fig. 3(e) & (f)), there are moist items (90.20Ω) and rock objects (775.46Ω). The MLP model has been successful in extracting the total number of major peaks and the corresponding waveform shapes in the model.

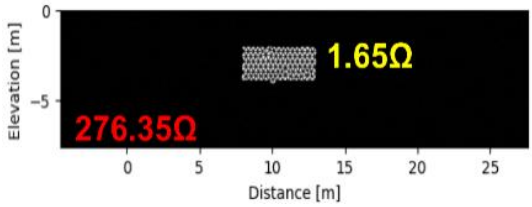

(a) Subsurface model with one anomaly object

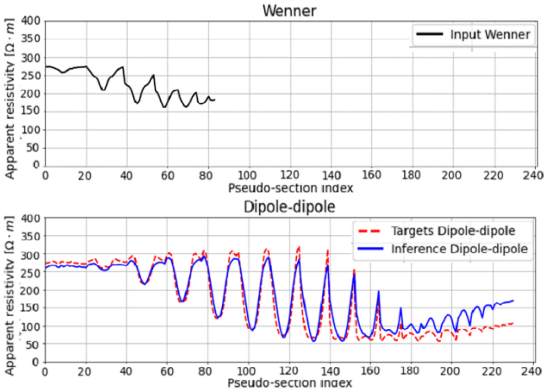

(b) Wenner input and Dipole-dipole target/inference results for model (a)

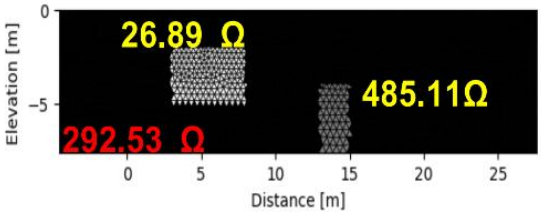

(c) Subsurface model with two anomaly objects

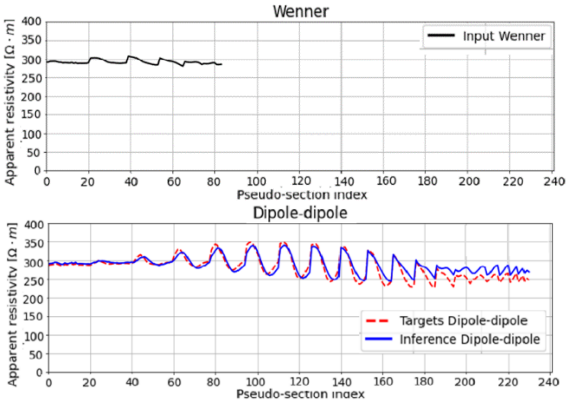

(d) Wenner input and Dipole-dipole target/inference results for model (c)

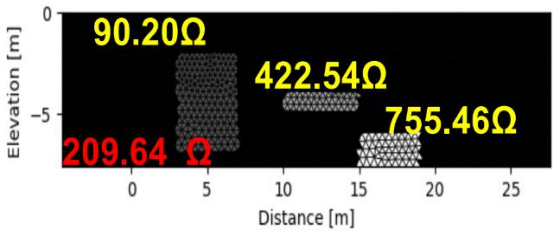

(e)Subsurface model with three anomaly objects

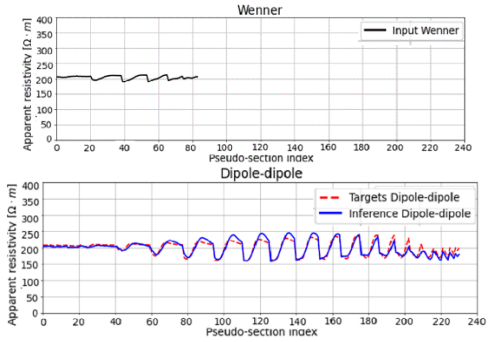

(f) Wenner input and Dipole-dipole target/inference results for model (e)

Fig 3. Inference results of the proposed MLP model for ground models with varying numbers of anomaly objects

However, as the level of interference and non-linear interactions among the objects intensified, some regions exhibited amplitude distortion and errors of position. This suggests that the resolution of the Wenner array's measurements cannot properly interpret the complexities of the subsurface structure, which may hamper the predictive ability of the trained model.

In other words, the inference model of deep learning, which is given only data from the Wenner array, has the capability of reproducing the spatial patterns of electric resistance just as the dipole-dipole arrangement would. In fact, it has good consistency when the scene is simple, featuring one object, and even when the scene becomes more complicated, the essential features are still traceable. In other words, the model has the capability of detecting the nonlinear changes in electric potential at boundaries of different materials in the ground.

5. Conclusion

The study proposes an MLP-based deep learning inference model that has the capability to make an accurate forecast of the dipole-dipole array response given data from a Wenner array. The model achieved excellent generalization performance with an R^2 of 0.9935 (±0.0014) with an RMSE of 3.44%, after being trained with 10,000 data samples and validated with an additional 1,000 data samples. The proposed model has excellent alignment with the actual dipole-dipole response. The residual plot gives evidence that there is no significant average deviation of the values of the targets and the values of the model output, which would serve as evidence of the reliability of the model's

inference. The targets have values of around 208.95 Ω·m, while the model output has values of around 208.98 Ω·m.

The proposed model combines the much more straightforward measurement characteristics of a Wenner array with the fine, high-resolution response of a dipole-dipole configuration. This represents a practical route toward approximating dipole-dipole-level responses through forward analysis alone, without complex inversion. Besides that, deep learning can handle naturally existing noise in data with ease, showcasing the power of achieving accurate analysis even in realistic situations.

Ultimately, the inference with deep learning that we have engineered could revolutionize the efficiency and usability of electrical resistivity surveys. The tool is ideally suited for practical, accurate ground truth assessments in the field, in the way one would identify areas where one would tip over with heavy construction equipment, for example. By making a software app that can automatically process real-time Wenner array data to produce a high-resolution dipole-dipole response, we have the capability to further integrate the system with measurement devices that alert users to areas prone to tipping over in real-time.

Declarations

Author Contributions

Conceptualization, L.B. and H.M.; methodology, L.B.; software, H.M.; validation, L.H., P.S. and H.M.; formal analysis, L.H.; investigation, H.M.; resources, L.B.; data curation, L.B.; writing original draft preparation, L.B.; writing review and editing, L.B.; visualization, P.S.; supervision, L.H.; project administration, L.H.; funding acquisition, L.H. All authors have read and agreed to the published version of the manuscript.

Acknowledgements

The authors would like to acknowledge the support provided by the School of Resources and Safety Engineering, Central South University, for providing the academic environment and facilities necessary for this research. The authors also thank the developers of ResIPy and the Python open source community for providing essential tools used in data simulation and analysis. Constructive discussions with colleagues during the course of this study are gratefully acknowledged. No additional external funding or non-author technical assistance was received for this work.

Conflict of Interest

The author declares that there are no potential conflicts of interest related to this paper.

References

[1] MILAZZO M.F., ANCIONE G., BRKIC V.S., and VALIS D. Investigation of crane operation safety by analyzing main accident causes. Risk, Reliability and Safety: Innovating Theory and Practice, 2017: 74–80. https://hdl.handle.net/11570/3121572

[2] HAMID A.R.A. et al. Causes of crane accidents at construction sites in Malaysia. IOP Conference Series: Earth and Environmental Science, 2019, 220(1): 012028. https://doi.org/10.1088/1755-1315/220/1/012028

[3] KIM S., and KANG C. Analysis of the complex causes of death accidents due to mobile cranes using a modified MEPS method. Sustainability, 2022, 14(5): 2948. https://doi.org/10.3390/su14052948

[4] CHOI S.K., BACK S.H., AN J.B., and KWON T.H. Geotechnical investigation on causes and mitigation of ground subsidence during underground structure construction. Journal of Korean Tunnelling and Underground Space Association, 2016, 18: 143–154.

[5] CHOI S.O. et al. Analysis of subsidence mechanism and development of evaluation program. Tunnelling and Underground Space, 2005, 15: 195–212.

[6] BURGER H.R., SHEEHAN A.F., and JONES C.H. Introduction to Applied Geophysics: Exploring the Shallow Subsurface. Cambridge University Press, Cambridge, 2023. https://doi.org/10.1017/9781316567418

[7] REYNOLDS J.M. An Introduction to Applied and Environmental Geophysics. John Wiley & Sons, Chichester, 1997.

[8] LOKE M.H., and BARKER R.D. Rapid least-squares inversion of apparent resistivity pseudosections using a quasi-Newton method. Geophysical Prospecting, 1996, 44(1): 131–152. https://doi.org/10.1111/j.1365-2478.1996.tb00142.x

[9] MENKE W. Geophysical Data Analysis: Discrete Inverse Theory. 3rd ed. Academic Press, Amsterdam, 2012. https://doi.org/10.1016/C2009-0-61848-4

[10] ASTER R.C., BORCHERS B., and THURBER C.H. Parameter Estimation and Inverse Problems. 3rd ed. Elsevier, Amsterdam, 2018. https://doi.org/10.1016/C2016-0-04931-3

[11] GUO Q., LIU B., WANG Y., and HE D. A Deep Learning Inversion Method for 3-D Electrical Resistivity Tomography Based on Neighborhood Feature Extraction. IEEE Sensors Journal, 2023, 23(16): 18550–18558. https://doi.org/10.1109/JSEN.2023.3293205

[12] ALEARDI M., VINCIGUERRA A., and HOJAT A. A convolutional neural network approach to electrical resistivity tomography. Journal of Applied Geophysics, 2021, 193: 104434. https://doi.org/10.1016/j.jappgeo.2021.104434

[13] PEREIRA J.L., and AZEVEDO L. Electrical resistivity tomography inversion combining deep variational autoencoder and stochastic adaptive

sampling. Geophysics, 2025, 90(2): E41–E50. https://doi.org/10.1190/geo2023-0456.1
[14] LOKE M.H. Electrical Imaging Surveys for Environmental and Engineering Studies: A Practical Guide to 2-D and 3-D Surveys. 1999. Available at: https://www.geotomosoft.com
[15] JANG H. et al. Preventing Overturning of Mobile Cranes Using an Electrical Resistivity Measurement System. Applied Sciences, 2024, 14: 9623. https://doi.org/10.3390/app14199623
[16] JANG H., and CHOI S. A Study on an Analytical Model for Preventing Overturning of Mobile Cranes Using Deep Learning. Journal of Drive and Control, 2024, 21(4): 231–238.
[17] RESIPY. ResIPy – Graphical User Interface for R2 family code, 2024. Available at: https://resipy.org
[18] PYTHON SOFTWARE FOUNDATION. Python Language Reference (Version 3.10.11), 2024. Available at: https://www.python.org
[19] HASTIE T., TIBSHIRANI R., and FRIEDMAN J. The Elements of Statistical Learning. 2nd ed. Springer, New York, 2009. https://doi.org/10.1007/978-0-387-84858-7
[20] NIELSEN M. Neural Networks and Deep Learning. Determination Press, 2015. http://neuralnetworksanddeeplearning.com
[21] GEMAN S., BIENENSTOCK E., and DOURSAT R. Neural networks and the bias/variance dilemma. Neural Computation, 1992, 4(1): 1–58. https://doi.org/10.1162/neco.1992.4.1.1
[22] SEONG B. et al. Predicting the spray uniformity of pest control drone using multi-layer perceptron. Journal of Drive and Control, 2023, 20(3): 25–34.
[23] JEONG H. et al. A Study of Weighing System to Apply into Hydraulic Excavator with CNN. Journal of Drive and Control, 2023, 20(4): 133–139.
[24] HOWARD A.G. et al. Mobile Nets: Efficient convolutional neural networks for mobile vision applications. arXiv preprint, 2017. https://arxiv.org/abs/1704.04861
[25] ABADI M. et al. TensorFlow: A system for large-scale machine learning. Proceedings of the 12th USENIX Symposium on Operating Systems Design and Implementation (OSDI 16), 2016: 265–283. https://www.usenix.org/conference/osdi16/technical-sessions/presentation/abadi
[26] LECUN Y., BENGIO Y., and HINTON G. Deep learning. Nature, 2015, 521: 436–444. https://doi.org/10.1038/nature14539.

参考文:

[1] MILAZZO M.F., ANCIONE G., BRKIC V.S., and VALIS D. 通过分析主要事故原因研究起重机作业安全. Risk, Reliability and Safety: Innovating Theory and Practice, 2017: 74–80. https://hdl.handle.net/11570/3121572
[2] HAMID A.R.A. et al. 马来西亚建筑工地起重机事故原因分析. IOP Conference Series: Earth and Environmental Science, 2019, 220(1): 012028. https://doi.org/10.1088/1755-1315/220/1/012028
[3] KIM S., and KANG C. 采用改进MEPS方法分析移动式起重机死亡事故的复杂原因. Sustainability, 2022, 14(5): 2948. https://doi.org/10.3390/su14052948
[4] CHOI S.K., BACK S.H., AN J.B., and KWON T.H. 地下结构施工过程中地面沉降原因及其缓解措施的岩土工程调查. Journal of Korean Tunnelling and Underground Space Association, 2016, 18: 143–154.
[5] CHOI S.O. et al. 地面沉降机理分析及评价程序开发. Tunnelling and Underground Space, 2005, 15: 195–212.
[6] BURGER H.R., SHEEHAN A.F., and JONES C.H. 应用地球物理学导论：浅层地下探测. Cambridge University Press, Cambridge, 2023. https://doi.org/10.1017/9781316567418
[7] REYNOLDS J.M. 应用与环境地球物理学导论. John Wiley & Sons, Chichester, 1997.
[8] LOKE M.H., and BARKER R.D. 基于拟牛顿法的视电阻率伪剖面快速最小二乘反演. Geophysical Prospecting, 1996, 44(1): 131–152. https://doi.org/10.1111/j.1365-2478.1996.tb00142.x
[9] MENKE W. 地球物理数据分析：离散反演理论. 第3版. Academic Press, Amsterdam, 2012. https://doi.org/10.1016/C2009-0-61848-4
[10] ASTER R.C., BORCHERS B., and THURBER C.H. 参数估计与反演问题. 第3版. Elsevier, Amsterdam, 2018. https://doi.org/10.1016/C2016-0-04931-3
[11] GUO Q., LIU B., WANG Y., and HE D. 基于邻域特征提取的三维电阻率层析成像深度学习反演方法. IEEE Sensors Journal, 2023, 23(16): 18550–18558. https://doi.org/10.1109/JSEN.2023.3293205
[12] ALEARDI M., VINCIGUERRA A., and HOJAT A. 基于卷积神经网络的电阻率层析成像方法. Journal of Applied Geophysics, 2021, 193: 104434. https://doi.org/10.1016/j.jappgeo.2021.104434
[13] PEREIRA J.L., and AZEVEDO L. 结合深度变分自编码器与随机自适应采样的电阻率层析成像反演方法. Geophysics, 2025, 90(2): E41–E50. https://doi.org/10.1190/geo2023-0456.1
[14] LOKE M.H. 环境与工程研究中的电成像测量：二维与三维测量实用指南. 1999. Available at: https://www.geotomosoft.com
[15] JANG H. et al. 基于电阻率测量系统的移动式起重机倾覆预防研究. Applied Sciences, 2024, 14: 9623. https://doi.org/10.3390/app14199623
[16] JANG H., and CHOI S. 基于深度学习的移动式起重机防倾覆分析模型研究. Journal of Drive and Control, 2024, 21(4): 231–238.
[17] RESIPY. ResIPy—R2 系列代码图形用户界面, 2024. Available at: https://resipy.org

[18] PYTHON SOFTWARE FOUNDATION. Python 语言参考手册 (Version 3.10.11), 2024. Available at: https://www.python.org
[19] HASTIE T., TIBSHIRANI R., and FRIEDMAN J. 统计学习要素. 第2版. Springer, New York, 2009. https://doi.org/10.1007/978-0-387-84858-7
[20] NIELSEN M. 神经网络与深度学习. Determination Press, 2015. http://neuralnetworksanddeeplearning.com
[21] GEMAN S., BIENENSTOCK E., and DOURSAT R. 神经网络与偏差—方差困境. Neural Computation, 1992, 4(1): 1–58. https://doi.org/10.1162/neco.1992.4.1.1
[22] SEONG B. et al. 基于多层感知机的病虫害防治无人机喷洒均匀性预测. Journal of Drive and Control, 2023, 20(3): 25–34.
[23] JEONG H. et al. 基于卷积神经网络的液压挖掘机称重系统研究. Journal of Drive and Control, 2023, 20(4): 133–139.
[24] HOWARD A.G. et al. MobileNets：用于移动视觉应用的高效卷积神经网络. arXiv preprint, 2017. https://arxiv.org/abs/1704.04861
[25] ABADI M. et al. TensorFlow：用于大规模机器学习的系统. Proceedings of the 12th USENIX Symposium on Operating Systems Design and Implementation (OSDI 16), 2016: 265–283. https://www.usenix.org/conference/osdi16/technical-sessions/presentation/abadi
[26] LECUN Y., BENGIO Y., and HINTON G. 深度学习. Nature, 2015, 521: 436–444. https://doi.org/10.1038/nature14539

Manuscript Information
Word count: 7,624 words (excluding references).

Peer-Review Record
Fast-track status: Not fast-tracked.
First-round reviews received: 3 reports.
Revision cycles completed: 3 rounds.
Final version submitted: March 8, 2026